

The STRIPAK component SipC is involved in morphology and cell-fate determination in the nematode-trapping fungus *Duddingtonia flagrans*

Valentin Wernet, Jan Wäckerle, and Reinhard Fischer*

Department of Microbiology, Institute for Applied Biosciences, Karlsruhe Institute of Technology (KIT)—South Campus, D-76131 Karlsruhe, Germany

*Corresponding author: Email: reinhard.fischer@KIT.edu

Homepage: www.iab.kit.edu

Abstract

The striatin-interacting phosphatase and kinase (STRIPAK) complex is a highly conserved eukaryotic signaling hub involved in the regulation of many cellular processes. In filamentous fungi, STRIPAK controls multicellular development, hyphal fusion, septation, and pathogenicity. In this study, we analyzed the role of the STRIPAK complex in the nematode-trapping fungus *Duddingtonia flagrans* which forms three-dimensional, adhesive trapping networks to capture *Caenorhabditis elegans*. Trap networks consist of several hyphal loops which are morphologically and functionally different from vegetative hyphae. We show that lack of the STRIPAK component SipC (STRIP1/2/HAM-2/PRO22) results in incomplete loop formation and column-like trap structures with elongated compartments. The misshapen or incomplete traps lost their trap identity and continued growth as vegetative hyphae. The same effect was observed in the presence of the actin cytoskeleton drug cytochalasin A. These results could suggest a link between actin and STRIPAK complex functions.

Keywords: striatin-interacting phosphatase and kinase (STRIPAK) complex; nematode-trapping fungi; *Duddingtonia flagrans*; fungal development; trap formation; septation

Introduction

Polar growth, polarity establishment, and maintenance of polarity of cells are common themes in biology and largely depend on cytoskeletal elements and functions. A *bona fide* example of polar growth is filamentous fungi with their extremely elongated hyphae (Riquelme *et al.* 2018). Most fungal species grow apically by continuous cell wall and cell membrane extension. Secretion vesicles containing, *e.g.*, cell wall biosynthesis enzymes are transported along microtubules (MTs) toward the tip, accumulate transiently in a so-called vesicle supply center or *Spitzenkörper* from where they are transported toward the apical membrane. After fusion with the membrane, they deliver their protein content (Riquelme *et al.* 2007). For the last travel distance, the actin cytoskeleton is required (Bergs *et al.* 2016; Schultzhaus *et al.* 2016). The MT and the actin cytoskeletons are coordinated through the action of so-called *cell-end marker proteins* at the cortex (Mata and Nurse 1997; Takeshita *et al.* 2013, 2014, 2017). Any variation from the tube-like morphology of hyphae is probably preceded and accompanied by cytoskeletal rearrangements.

One intriguing fungal hyphal morphology is the ring-like structure of traps of nematode-trapping fungi (NTF) (Jiang *et al.* 2017). These fungi can switch from a saprotrophic to a predatory lifestyle under low-nutrient conditions and in the presence of nematodes. More than 200 NTF have been identified and many are found in the Orbiliaceae (Ascomycota). A wide range of

morphologically different traps are produced by different species, ranging from adhesive knobs and columns, adhesive trap rings and networks, and constricting and non-constricting rings (Su *et al.* 2017). One of the best-studied NTF at the molecular level is *Arthrobotrys oligospora*, where also the signal exchange between fungus and nematodes and the control of trap formation were studied (Niu and Zhang 2011; Hsueh *et al.* 2013, 2017; Yu *et al.* 2021). In the case of *Duddingtonia flagrans*, a close relative of *A. oligospora*, ring-like, adhesive traps are formed, in which *Caenorhabditis elegans* or other nematodes are captured (Youssar *et al.* 2019). The ring-like morphology of the traps is rather unique and requires a redirection of the polarity axis, cell-cell recognition, and hyphal fusion. This morphological differentiation goes along with physiological differentiation, the production of adhesives, and the preparation for the penetration of caught nematodes. Another fascinating aspect is the determination of the size of the traps. They should have a defined diameter to effectively catch nematodes. If they are too large, nematodes could slip through, and if the diameter is too small, nematodes will not be able to enter the traps. Size determination probably also requires a functional cytoskeleton. How these fascinating morphological changes are initiated and which signaling modules are required are largely unknown.

Although some trapping-deficient mutants have been identified in *A. oligospora*, the molecular basis and cell biology of trap

Received: May 26, 2021. Accepted: August 20, 2021

© The Author(s) 2021. Published by Oxford University Press on behalf of Genetics Society of America.

This is an Open Access article distributed under the terms of the Creative Commons Attribution License (<https://creativecommons.org/licenses/by/4.0/>), which permits unrestricted reuse, distribution, and reproduction in any medium, provided the original work is properly cited.

morphogenesis are poorly understood (Kuo et al. 2020; Chen et al. 2021). Recently, a random mutagenesis analysis identified 15 mutants with deficiencies in trap morphogenesis. However, there are still difficulties in gene mapping because of heterokaryotic transformants and the lack of genetic crosses of NTF (Huang et al. 2021). In *D. flagrans*, it was shown that a cell dialog between the tip trap cell and the basal cell is required for ring closure (Youssar et al. 2019).

The early stages of trap formation in *D. flagrans* resemble the spiral growth of ascogonia or crozier formation of ascomycetes during sexual development (Read and Beckett 1996). An ascogenous hypha elongates and bends over to form a hook-shaped structure. In *Sordaria macrospora*, a genetic screen has identified several “pro” mutants with defects in sexual development, and some PRO proteins are components of the striatin-interacting phosphatase and kinase (STRIPAK) complex (Stein et al. 2020; Teichert et al. 2020). The STRIPAK complex is a highly conserved eukaryotic signaling module responsible for the regulation of numerous cellular and developmental processes. It was initially identified in mammals, where it was linked to human diseases like Alzheimer’s, diabetes, and cardiac diseases (Goudreault et al. 2009; Hwang and Pallas 2014). Recently, the structure of the human STRIPAK core was solved by cryo-EM (Jeong et al. 2021). The serine–threonine protein phosphatase 2 (PP2A) core enzyme consists of a scaffold subunit A (PP2A), the catalytic subunit C (PP2AC), and a regulatory subunit of the B''' (striatin) family. In addition, multiple subunits are associated with the core subunits of the phosphatase, including the striatin-interacting protein 1 or 2 (STRIP1 or STRIP2), the monopolar spindle one-binder (Mob) protein Mob3, cerebral cavernous malformation 3, the sarcolemmal membrane-associated protein (SLMAP), and the coiled-coil protein suppressor of IκB kinase-ε. Furthermore, various germinal center kinases (GCKs) are associated with the STRIPAK complex for enhanced regulation.

The STRIPAK complex is involved in the regulation of key cellular processes including signaling, cytoskeletal organization, cell cycle control, cell migration, cell polarity, apoptosis, Golgi assembly, cell morphology, and vesicular trafficking (Hwang and Pallas 2014; Kück et al. 2019). In *Drosophila melanogaster*, it was shown that the STRIPAK complex is a negative regulator of the Hippo signaling pathway through its phosphatase activity (Ribeiro et al. 2010). RNAi screening identified the STRIP1/2 orthologs FAM40A and FAM40B to affect cell shape in *Drosophila* S2 cells (Rohn et al. 2011). In an RNAi screening in PC3 prostate cancer cells, FAM40A-depleted cells were flattened with high levels of cortical F-actin compared to the control, whereas FAM40B-depleted cells were elongated with long thin protrusions (Bai et al. 2011). In *Saccharomyces cerevisiae*, the STRIPAK homolog Factor arrest protein complex (Far complex) is involved in pheromone-induced cell cycle arrest and affects signaling through the target of rapamycin complex 2 (Kemp and Sprague 2003; Pracheil et al. 2012). In *Schizosaccharomyces pombe*, the STRIPAK homologous Septation initiation network (SIN) Inhibitory PP2A complex (SIP) negatively regulates SIN and is important for coordinating mitosis and cytokinesis (Singh et al. 2011; Simanis 2015).

Functional analyses in filamentous fungi revealed that different components are required for cell–cell fusion, sexual fruiting body development, septation, secondary metabolite production, symbiotic interactions, and pathogenicity (Xiang et al. 2002; Pöggeler and Kück 2004; Green et al. 2016; Zhang et al. 2018; Elramli et al. 2019). But only recent proteomic and phosphoproteomic studies in *S. macrospora* revealed an extended signaling

network that is modulated by the STRIPAK complex (Märker et al. 2020).

Here, we studied the STRIPAK complex in the NTF *D. flagrans*, investigated the role of the STRIPAK complex component SipC/STRIP1/2 during septation and the unique hyphal ring formation during trap morphogenesis, and found that SipC is involved in cell-fate determination.

Material and methods

Strains and culture conditions

D. flagrans strains were cultivated at 28°C on potato dextrose agar (PDA; Carl Roth). All fungal strains used in the study are listed in Table 1.

To induce trap formation, the fungal strains were cultivated on thin low-nutrient agar (LNA) slides by adding around 1×10^4 *D. flagrans* spores and around 100–500 *C. elegans* individuals. Co-incubation was carried out at 28°C in darkness for 12–48 h. *C. elegans* strains were cultivated at 20°C on nematode-growth medium seeded with *Escherichia coli* strain OP50 as food source.

Targeted gene deletion of sipC

sipC was deleted by homologous recombination. One kb flanks homologous to the 5' and 3' regions of sipC were amplified by PCR with primers with 25 bp overhangs homologous to the hygromycin-B resistance cassette as well as to the pJET1.2 plasmid backbone (Thermo Fisher), digested with EcoRV (Tables 2 and 3). The hygromycin-B resistance cassette hph was amplified using plasmid pFC332 as template, and all fragments were assembled into pJET1.2 using the NEBuilder HiFi DNA Assembly Cloning Kit [New England Biolabs (NEB), Frankfurt]. The fragments were amplified using Q5 polymerase (NEB) and the manufacturer’s recommended protocol. Standard protocols were used for *E. coli* transformation and plasmid isolation. The gene deletion construct was introduced into *D. flagrans* protoplasts as described in Youssar et al. (2019). For selection of transformants, PDA plates supplemented with 100 µg/ml hygromycin-B were used. To reintroduce the full-length target gene into the deletion strains, the whole gene including its 1 kb upstream and 0.5 kb downstream regulatory regions was amplified by PCR. To select for positive

Table 1 *D. flagrans* strains used in this study

Strain		Reference
WT	CBS 349.94	CBS-KNAW
sVW03	sipC::hph (ΔsipC); trpC(p)::hph::trpC(t)	This study
sVW05	ΔsipC; sipC(p)::sipC::sipC(t); gpdA(p)::neo::trpC(t)	This study
sVW10	h2b(p)::h2b::GFP::h2b(t); gpdA(p)::neo::trpC(t)	This study
sVW15	ΔsipC; tubA(p)::mCherry::tubA::tubA(t); gpdA(p)::neo::trpC(t)	This study
sVW16	ΔsipC; tubA(p)::lifeact::GFP::gluC(t); gpdA(p)::neo::trpC(t)	This study
sVW18	tubA(p)::mCherry::tubA::tubA(t); trpC(p)::hph::trpC(t)	This study
sVW22	ΔsipC; h2b(p)::h2b::GFP::h2b(t); gpdA(p)::neo::trpC(t)	This study
sVW24	sVW10 + sipC(p)::h2b::mCherry::h2b(t); trpC(p)::hph::trpC(t)	This study
sVWZ	tubA(p)::lifeact::GFP::gluC(t); trpC(p)::hph::trpC(t)	This study
sVW X	p12(p)::p12::mCherry::gluC(t); trpC(p)::hph::trpC(t)	This study
sVW Y	ΔsipC; p12(p)::p12::mCherry::gluC(t); gpdA(p)::neo::trpC(t)	This study

Table 2 Plasmids used in this study

Name	Description	Reference
pVW28	<i>sipC::hph (ΔsipC)</i>	This study
pJW04	<i>h2b(p)::h2b::GFP::h2b(t); gpdA(p)::neo::trpC(t)</i>	This study
pVW37	<i>sipC(p)::sipC::sipC(t); trpC(p)::neo::trpC(t)</i>	This study
pVW41	<i>lifeact::GFP</i>	This study
pVW42	<i>tubA(p)::lifeact::GFP; trpC(p)::hph::trpC(t)</i>	This study
pVW56	<i>p12(p)::h2b::mCherry::gluC(t); trpC(p)::hph::trpC(t)</i>	This study
pVW57	<i>tubA(p)::mCherry::tubA::tubA(t); trpC(p)::hph::trpC(t)</i>	This study
pVW70	<i>sipC(p)::h2b::mCherry::h2b(t); trpC(p)::hph::trpC(t)</i>	This study
pVW77	<i>tubA(p)::mCherry::tubA::tubA(t); gpdA(p)::neo::trpC(t)</i>	This study
pVW78	<i>tubA(p)::lifeact::GFP; gpdA(p)::neo::trpC(t)</i>	This study
pVW114	<i>p12(p)::p12::mCherry::gluC(t); trpC(p)::hph::trpC(t)</i>	This study
pVW115	<i>p12(p)::p12::mCherry::gluC(t); gpdA(p)::neo::trpC(t)</i>	This study
pIH02	<i>pplasmid backbone containing trpC(p)::hph::trpC(t)</i>	Youssar et al. (2019)
pJM16	<i>plasmid backbone containing gpdA(p)::neo::trpC(t)</i>	J. Menzner, KIT
pNH20	<i>plasmid backbone containing tubA(p); trpC(p)::hph::trpC(t)</i>	N. Wernet, KIT

Table 3 Oligonucleotides used in this study

Name	Sequence (from 5' to 3')	Description
pro22_ko_LB_fwd	GATGGCTCGAGTTTTTCAGCAAGATCGATGCCTAACTGATATGGTAG	ΔsipC
pro22_ko_LB_rev	GTTGACCTCCACTAGCATTACACTTTTTGATGGTATATTTGGGAGGTG	ΔsipC
pro22_ko_hph_fwd	ACCACCTCCCAAATATACCATCAAAAAGTGTAATGCTAGTGGAGGTC	ΔsipC
pro22_kp_hph_rev	GGGTCCGACCTTCTGGCCCTCGTTTTGGGGGGAGTTTAGGGAAAAG	ΔsipC
pro22_ko_RB_fwd	ATGCTCTTTCCCTAAACTCCCCCAAACGAGGGCCAGAAGGTGG	ΔsipC
pro22_ko_RB_rev	ATTGTAGGAGATCTTCTAGAAAAGATCCAGTTTGTGAGGTGCTAAAC	ΔsipC
pro22_rek_prom_fwd	GATGGCTCGAGTTTTTCAGCAAGATCGAAACTTCTCTGGAAGCGA	ΔsipC complementation
pro22_term_rev	GTTGACCTCCACTAGCATTACACTTCCAGTTTGTGAGGTGCTAAAC	ΔsipC complementation
pro22_g418_fwd	GTCCGTTTAGCACCTGACAAACTGGAAGTGAATGCTAGTGGAGGT	ΔsipC complementation
pro22_g418_rev	ATTGTAGGAGATCTTCTAGAAAAGATTGGGGGGAGTTTAGGGAAA	ΔsipC complementation
tubP_hphol_fwd	TGCTCTTTCCCTAAACTCCCCCAGTAGCTGCCAGCAAACCTC	mCherry-TubA
tubP_RFPol_rev	TACTTACCTCGCCCTTGCTTACCATGATGAATTATATTTTCGTCGAAGAAGA	mCherry-TubA
RFP_tubPol_fwd	TCTTCTTGACGAAATATAAATTCATCATGTTGTAAGCAAGGGCCGAGG	mCherry-TubA
RFP_tubAol_rev	CGTTGATAGAAACAACCTTCACGCATTTTGTAGAGTTCATCCATTCCAC	mCherry-TubA
TubA_RFPol_fwd	CGGTGGAATGGATGAACTCTACAAAATGCGTGAAGTTGTTTCTATCAAC	mCherry-TubA
Df_tubA_term_rev	ATTGTAGGAGATCTTCTAGAAAAGATATACCGTGTGGCTGCCGAA	mCherry-TubA
lifeact_botgfp_fwd	ATGGCGTGGCCGACCTGATCAAGAAGTTCGAGAGCATCAGCAAGGAAG- AGATGGTTTCCAAGGGTGAGG	Lifeact-GFP
df_tub_rev	TGCAATTGTTGATGTTCAGGC	Lifeact-GFP
tg_luc_fwd	CGTATGTAGATAAGATGTATGATTAG	Lifeact-GFP
lifeact_tubOL_fwd	GAAAGCCTGAACATCAACAATTGCAATTGGGCGTGGCCGACCT	Lifeact-GFP
gfp_cterm_tglucol_rev	AATCATACATCTTATCTACATACGTTATTTGTAAGTTTCATCCATTCCCA	Lifeact-GFP
p12_lb_hph_ol_fwd	ATGCTCTTTCCCTAAACTCCCCCAGAGCAGCTCCGAAAGCAAAG	P12-mCherry
p12_ns_mch_ol_rev	TACTTACCTCGCCCTTGCTTACCATAGTGTGCGAAGTGTAGCCG	P12-mCherry

transformants, the geneticin resistance cassette [*trpC(p)::neo::trpC(t)*] was used. Both fragments were assembled into the pJET1.2 plasmid backbone using the NEBuilder HiFi DNA Assembly Cloning Kit. The complementation plasmid was introduced into the respective mutant strain via protoplast transformation. For selection of transformants, PDA plates supplemented with 150 μg/ml geneticin sulfate (G418) were used.

Verification of homologous recombination

To extract genomic DNA from *D. flagrans*, around 1×10^8 spores were inoculated in potato dextrose broth and incubated in a 6-cm diameter Petri dish at 28°C for 48 h. Afterward, the mycelium was collected, and DNA was extracted using the protocol described in Zhou et al. (2018). Southern blot analysis was done with digoxigenin (DIG)-labeled probes. Genomic DNA was digested with the appropriate restriction enzyme overnight, separated in a TAE agarose gel and transferred to a nylon membrane. Probes were synthesized using the PCR DIG Probe Synthesis Kit (Roche)

according to the manufacturer's protocol. After probe hybridization, the membrane was hybridized with anti-DIG-AP Fab fragments (Roche) and development was performed using CDP-Star solution (Roche).

Localization of proteins with GFP and mCherry

mCherry-TubA: TubA was tagged with mCherry at the N-terminus expressed from the natural promoter. Using Gibson assembly, PCR-amplified fragments of the hygromycin resistance cassette *hph*, 1 kb *tubA* promoter, *GFP*, and *tubA* open reading frame plus 1 kb downstream regulatory region were cloned into a pJET1.2 plasmid backbone. To express the construct in *D. flagrans* mutant strains, the *tubA(p)::mCherry::tubA::tubA(t)* fragment was cloned into pJM16 containing the G418 resistance cassette. Plasmids and oligonucleotides are listed in Tables 1 and 2.

Lifeact-GFP: Lifeact was tagged with GFP at the C-terminus expressed from the *tubA* promoter (Tables 1 and 2). The 51-bp

sequence coding for lifeact was included in the forward primer to amplify GFP and subcloned into a pJET1.2 plasmid backbone. Using Gibson assembly, the PCR-amplified Lifeact-GFP fragment was cloned into pNH20 containing the *tubA* promoter and a hygromycin-B resistance cassette. To express the construct in *D. flagrans* mutant strains, the *tubA(p)::lifeact::gfp::gluC(t)* fragment was cloned into pJM16 containing the G418 resistance cassette.

Transcription reporter assay

To localize the expression of *sipC* in *D. flagrans* during different developmental stages, the *sipC* promoter was fused to the fluorescent reporter gene construct *h2b-mCherry*. The promoter fragment was amplified by PCR and assembled into the plasmid backbone pVW56 containing the *h2b::mCherry* reporter and the hygromycin-B resistance cassette by Gibson assembly. The plasmid was transformed into *D. flagrans* sVW10 expressing *h2b(p)::h2b::GFP*.

Quantification of compartment length, conidiation, and trap morphogenesis

To quantify compartment length of vegetative mycelium, around 1000 spores of the respective *D. flagrans* strain were inoculated on LNA at 28°C for 24 h. The cell wall was stained with Calcofluor White and images were taken at 100× magnification. For each strain, the length of ten compartments of five germinated spores was quantified and performed in three replicates.

To quantify the amount of conidia produced by the different *D. flagrans* strains, 8-mm diameter hyphal discs were punched from the edges of a 7-day-old cultured PDA plate, transferred into 500 µl dH₂O, and vortexed for 5 min. Conidia were quantified using a Helber counting chamber. Each biological replicate was quantified four times. To quantify chlamydospore quantities and morphology in the $\Delta sipC$ strain, 1000 spores of wild type (WT), $\Delta sipC$, and rescue strain were incubated on LNA at 28°C. After 72 h, chlamydospore number and morphology were assessed. To quantify the morphology of fungal traps, around 1000 spores of the respective *D. flagrans* strains were co-inoculated with around 200 *C. elegans* larvae on thin LNA pads (2 × 2 cm) at 28°C for 48 h. The traps were counted and quantified using 100× and 400× magnification. For each strain, three biological replicates were quantified.

Microscopy

For microscopy, around 1×10^4 spores were inoculated on thin LNA (1% agar 1.66 mM MgSO₄, 5.4 µM ZnSO₄, 2.6 µM MnSO₄, 18.5 µM FeCl₃, 13.4 mM KCl, 0.34 µM biotin, and 0.75 µM thiamin) and incubated for at least 2 h at 28°C. For conventional fluorescence images, a Zeiss AxioImager Z.1 microscope with either Plan-Apochromat 63×/1.4 Oil DIC, EC Plan-Neofluar 40×/0.75, EC Plan-Neofluar 20×/0.50, or EC Plan-Neofluar 10×/0.30 objective and an AxioCamMR was used. The images were taken using ZEN 2012 Blue Edition.

For confocal imaging, a Zeiss LSM900 microscope with Plan Apochromat 63×/1.4 Oil objective and Airyscan 2 detector in super resolution mode was used.

Fluorescent dyes and inhibitors

To visualize the cell wall of the fungus, the mycelium was stained using Calcofluor-white (CFW, fluorescent brightener 28; Sigma-Aldrich). The 1% (wt/vol) stock solution was prepared by dissolving CFW in 0.5% (wt/vol) KOH and 83% (vol/vol) glycerol. A 1:1000 dilution working solution (in dH₂O) was added to the mycelium and incubated for 3 min to stain the cell wall before imaging.

A stock solution (1 mg/ml) of the anti-MT agent methyl 1-(butylcarbamoyl)-2-benzimidazolecarbamate (benomyl; Sigma) was prepared in dimethyl sulfoxide (DMSO) and used at a final working concentration of 5 µg/ml in dH₂O. A stock solution (1 mg/ml) of the F-actin depolymerizing drug Cytochalasin A was prepared in DMSO and used at a final working concentration of 5 µg/ml in dH₂O. For the inhibitors, a 0.5 × 0.5-cm agar pad with mycelium was incubated in 100 µl working solution of each inhibitor and incubated for up to 60 min prior to imaging.

Statistical analysis

P-values were calculated using the mean of three biological replicates and the t-test with the software GraphPad Prism 9. In the bar graphs, each biological replicate is color-coded (orange, blue, gray). While each data point is depicted as dot, the averages are shown as triangles (Lord et al. 2020).

Results

Conservation of the STRIPAK signaling complex in *Duddingtonia flagrans*

To unravel a role of the STRIPAK complex in trap formation, we identified orthologs of *S. macrospora* PRO11, PP2AA, PP2Ac1, PRO22, SmMOB3, PRO45, SmKIN3, SmKIN24, and SC11 in *D. flagrans* (Figure 1). They all share conserved domains with homologs from other fungi, suggesting that *D. flagrans* harbors a functional STRIPAK complex. In *A. nidulans*, the STRIPAK complex consists of the striatin scaffold protein StrA and six striatin (StrA) interacting proteins (Sip), and the heptameric complex is involved in the regulation of light-dependent development, the production of secondary metabolites, and the stress response (Elramli et al. 2019). We followed the nomenclature of *A. nidulans* for the *D. flagrans* STRIPAK proteins and named the proteins striatin StrA and StrA-interacting proteins (SipA-F). StrA [DFL_002622; 764 amino acids (aa)] contains a conserved striatin domain consisting of a caveolin-binding domain and a calmodulin-binding domain. Additionally, it contains WD40 repeats at the C-terminus. SipA (DFL_000993; 426 aa) is an ortholog of Mob3 (Phocein) containing the conserved Mob1-Phocein domain. The ortholog of STRIP1/2 SipC (DFL_007682; 1010 aa) harbors the putative N1221 family domain and a domain of unknown function (DUF3402). The SLMAP protein SipD (DFL_001177; 744 aa) harbors a forkhead-associated (FHA) domain. The ortholog of the catalytic subunit of the phosphatase PP2Ac SipE (DFL_003255; 313 aa) contains the catalytic domain of protein phosphatase 2A. The ortholog of the phosphatase regulatory subunit PP2AA SipF (DFL_008478; 619 aa) contains HEAT repeats (Huntingtin, elongation factor 3, protein phosphatase 2A, and the yeast kinase TOR1). Two putative STRIPAK-associated GCKs DFL_002427 and DFL_007266 were identified. No ortholog for SipB was found.

STRIPAK *sipC* expression

As a first step to characterize the functions of the STRIPAK complex in *D. flagrans*, we analyzed the *sipC* gene. The open reading frame comprises 3528 nucleotides and is disrupted by nine introns [confirmed by RNAseq data (Youssar et al. 2019)]. To test if the expression levels change in different hyphae, a microscopical reporter assay was used. To this end, we fused the *sipC*-promoter to the fluorescent reporter gene *mCherry* which was further linked to the histone *h2b* gene (*h2b*), resulting in red fluorescent nuclei when the promoter is active (Yu et al. 2021). As a control, the fluorescent reporter gene *h2b-GFP* was expressed with the *h2b*-promoter. The overall expression of *sipC* was weak. No fluorescence

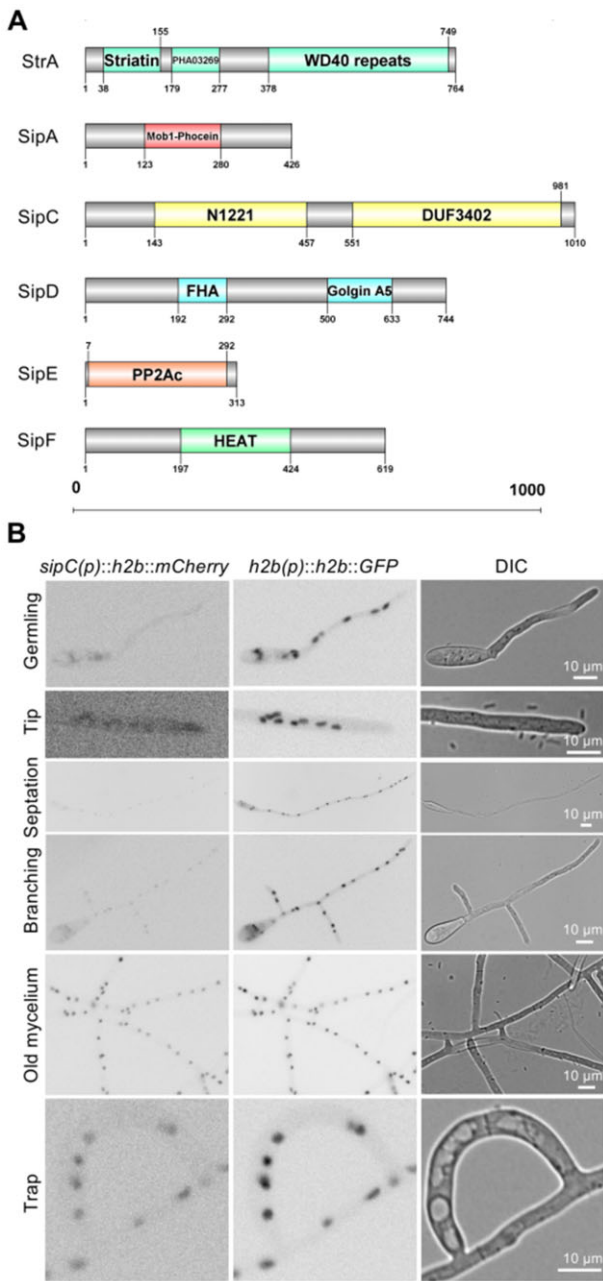


Figure 1 Scheme of *D. flagrans* STRIPAK orthologs and expression of *sipC* in hyphae and traps. (A) Domain organization of *D. flagrans* STRIPAK components. The amino acids are numbered, and conserved domains are labeled. Abbreviations: WD40, WD or beta-transducin repeat sequence; FHA, forkhead-associated; HEAT, Huntingtin, elongation factor 3, protein phosphatase 2A, and the yeast kinase TOR1; Mob1, monopolar spindle one-binder protein; N1221, acidic domain with possible transmembrane domains; DUF3402, domain of unknown function 3402; PHAO3269, envelope glycoprotein C. (B) Visualization of the expression of *sipC* using a H2B-mCherry reporter construct. The expression of *h2b-GFP* under the *h2b* promoter was used as a control. Exposure time: mCherry 300 ms, GFP 200 ms. Fungal germlings were observed after 1–2 h of incubation on LNA. Old mycelium refers to at least 16 h postinoculation of spores.

was observed in early stages, 4 h after germination of conidiospores, or in the first 10–30 μm of the hyphae (Figure 1B). Fluorescence started to appear in nuclei when the first septum or hyphal branches became visible. Higher levels of expression were

observed in older parts of the mycelium (16 h incubation). During trap formation, no significant changes in expression were detected, and the fluorescence of the reporter construct resembled the intensity of later-stage mycelium. These results suggest a function after germ-tube formation during hyphal differentiation.

sipC is required for fast vegetative growth and septation

Since *sipC* was expressed during septum formation, we next generated a *sipC*-deletion strain by replacing the gene with a hygromycin-B resistance cassette by homologous recombination. Twenty-nine hygromycin-B resistant transformants were obtained and screened by PCR and Southern blot analysis. One transformant showed the expected integration and was used for further studies (Figure 3A).

Deletion of *sipC* resulted in slow-growing colonies. While the WT completely covered the medium on a 9-cm Petri dish in 7 days when center inoculated, the ΔsipC mutant needed around 21 days (Figure 3B). The formation of aerial mycelium is a common feature of *D. flagrans* on PDA medium. In the ΔsipC -deletion strain, it was restricted to the first 1–2 cm of the initial inoculation site. Additionally, the ΔsipC mutant showed a 1-cm ring-like growth pattern on PDA. The mutant phenotype could be fully re-complemented with an ectopic copy of the *sipC* gene, including 1 kb upstream and 0.5 kb downstream regulatory elements.

Since we observed the start of expression of *sipC* during septum formation, we quantified the number of septa in the ΔsipC -deletion strain after inoculating spores on a low-nutrient medium and incubation for 24 h (Figure 3C). Generally, growth of the ΔsipC strain was slower in comparison to the WT and the respective re-complementation strain. While hyphal compartments in WT and the re-complemented mutant strain had a length of $48.5 \pm 5 \mu\text{m}$ [mean standard deviation (SD)] and $42.6 \pm 0.3 \mu\text{m}$, respectively ($n = 150$), the compartment size was doubled in the ΔsipC -deletion strain with a length of $102 \pm 5 \mu\text{m}$. The differences were still present after an additional 24 h of incubation, resulting in decreased numbers of septa compared to WT. In the ΔsipC -deletion strain, septa were mainly found at branching points. Interestingly, whereas the Δpro22 mutant in *S. macrospora* and $\Delta\text{ham-2}$ mutant in *Neurospora crassa* failed to undergo cell–cell fusion (Xiang et al. 2002; Bloemendal et al. 2010), in the *D. flagrans* ΔsipC -deletion strain, the process appeared unaffected (Figure 3D). The frequency of hyphal fusion in the ΔsipC -deletion strain was difficult to compare to WT, since growth speed was heavily reduced.

SipC is required for asexual development and determines chlamydospore morphology

Deletion of *sipC* heavily influenced the number of asexual conidia production, resulting in an 80% reduction of conidia of 7-day-old cultures compared to WT (Figure 4A). Likewise, the amount of chlamydospores produced after 72 h on LNA was reduced by 88% compared to WT. In addition, the morphology of chlamydospores was drastically altered, with $71 \pm 3\%$ highly elongated and expanded spores in the mutant ($n = 3$) (Figure 4, C–E). All chlamydospores of the WT had a round shape with an average diameter of $22.7 \pm 0.5 \mu\text{m}$ compared to the chlamydospores of the ΔsipC -deletion strain which had a length of $33.9 \pm 0.7 \mu\text{m}$. Yet, these spores were still able to germinate. Chlamydospores develop from differentiated vegetative hyphae, while conidia are formed at the tip of conidiophores. Chlamydospores are formed in older mycelium by

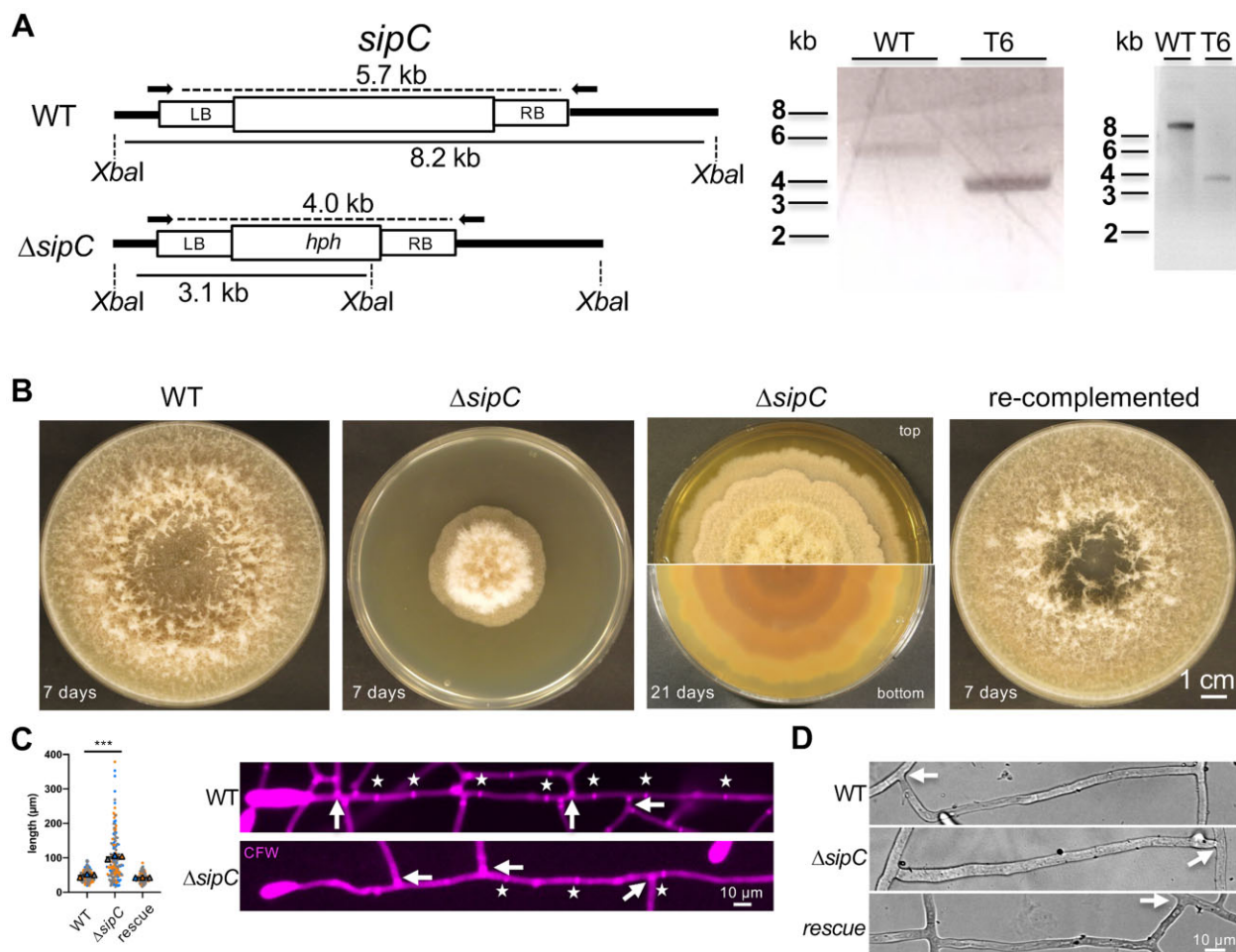


Figure 2 Deletion of *sipC* impairs vegetative growth and septation. (A) Targeted deletion of the *sipC* gene in *D. flagrans* using homologous recombination. Left: scheme of the deletion strategy. Right: analytic PCR using primers indicated on the left (as arrows) and southern blot analysis (outer right panel) using the probe indicated in the scheme. Genomic DNA of wild type (WT) and transformant no. 6 (T6) was digested with *XbaI* before blotting and hybridizing. (B) Growth of *D. flagrans* WT, the $\Delta sipC$ mutant T6, and the re-complemented strain on PDA after 7 days. Additionally, top and bottom view of the $\Delta sipC$ mutant on PDA after 21 days are shown. (C) Septation of vegetative mycelium in WT, the $\Delta sipC$ mutant, and the re-complemented strain. Septa were stained with Calcofluor White. Asterisks indicate septa of the main hyphae. Arrows indicate septa at branching hyphae. Quantification of compartment length in each strain. Each biological replicate is color-coded (orange, blue, gray). While each data point is depicted as dot, the averages are shown as triangles. Error bars show the standard deviation (SD). (D) Hyphal fusion events in WT, $\Delta sipC$, and the re-complemented strain are labeled with white arrows.

condensing the cytoplasm within a compartment into a thick-walled spore. This formation is rather difficult in the $\Delta sipC$ -deletion strain since the compartment size is much larger than in WT.

SipC determines the fate of trap cells

To investigate trap morphogenesis of the $\Delta sipC$ -deletion strain, *C. elegans* was co-incubated with fungal spores on LNA slides for at least 48 h. While trap formation in WT and the re-complemented strain showed ring-like trap networks, this was heavily disturbed in the $\Delta sipC$ -deletion mutant (Figure 5A). Trap loops were often incomplete and resulted in column-like structures. These column-like traps were either identified and distinguished from normal vegetative hyphae by comparing the hyphal diameter or by an increased fluorescence after CFW staining (Figure 5B). An already formed trap can be a new starting point for another trap resulting in more complex trapping networks. Compared to WT,

this phenomenon was restricted in the $\Delta sipC$ mutant (Figure 5C). Trap morphology was restored in the re-complemented strain (Figure 5D). The number of nuclei in trap cells in WT and the $\Delta sipC$ -deletion mutant strain showed no apparent difference (Figure 5E).

Traps of the $\Delta sipC$ -deletion strain were divided into four groups according to the morphology of the trap, and the occurrence was quantified (Figure 6A). Of all counted traps, $77 \pm 2\%$ showed a column-like structure (I), $13 \pm 3\%$ a ring-like structure without cell fusion (II), $8 \pm 1\%$ a 90 degrees bending (III), and $1 \pm 1\%$ a ring with cell fusion (IV) appearance (total trap number in three biological replicates were $n = 224$, $n = 156$, and $n = 276$, respectively; Figure 6B). In contrast, mostly traps of group II and IV occurred in WT and the re-complemented strain. Despite the morphological differences, traps of the $\Delta sipC$ -deletion strain were still adhesive, and the strain was able to immobilize and digest nematodes (Figure 7A).

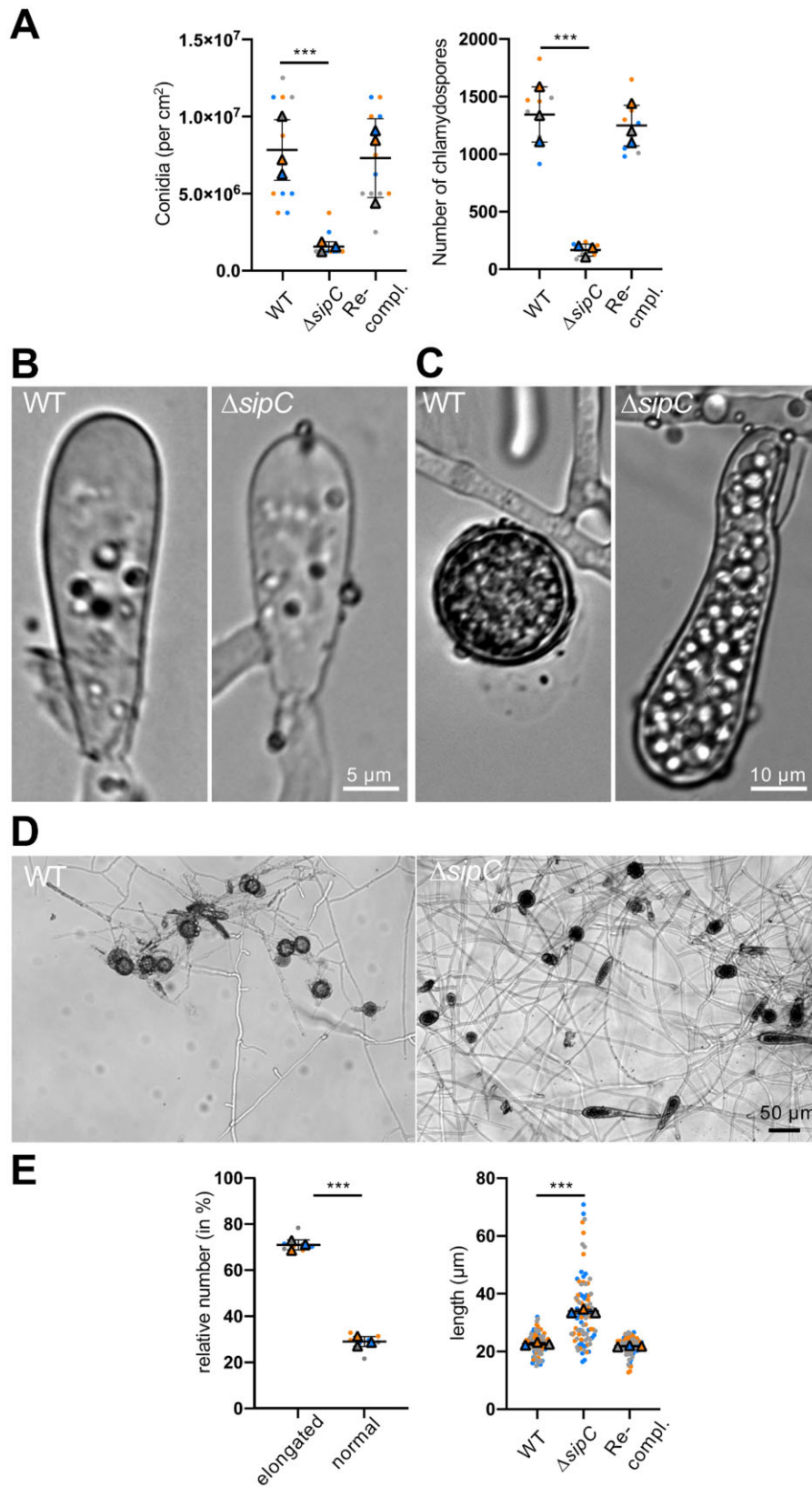


Figure 3 SipC is required for asexual development and determines chlamydo-spore morphogenesis. (A) Quantification of the number of conidia and chlamydo-spores in WT, the $\Delta sipC$ mutant, and the re-complemented strain. (B) Microscopic pictures of conidia of the WT and the $\Delta sipC$ -mutant strain. (C) Microscopic pictures of chlamydo-spores of the WT and the $\Delta sipC$ -mutant strain. (D) Overview of chlamydo-spores of the WT and the $\Delta sipC$ -mutant strain. (E) Quantification of chlamydo-spore morphology in the $\Delta sipC$ strain and quantification of chlamydo-spore length of the WT, the $\Delta sipC$ mutant, and the re-complemented strain. Each biological replicate is color-coded (orange, blue, gray). While each data point is depicted as dot, the averages are shown as triangles. Error bars show the SD.

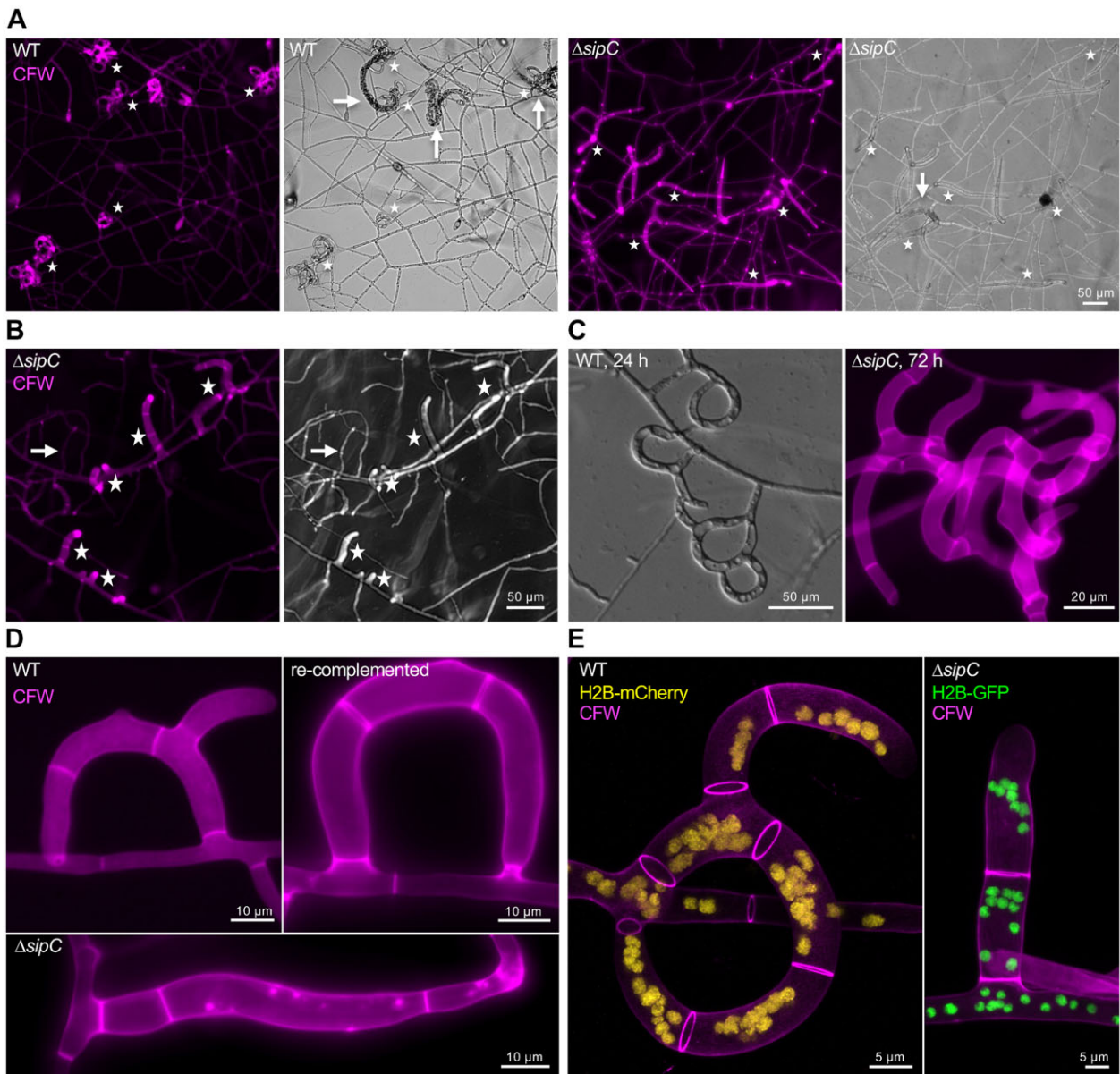


Figure 4 SipC is required for trap formation. (A) Comparison of trap formation in WT, the $\Delta sipC$ mutant, and the re-complemented strain. The asterisks indicate traps. Trapped *C. elegans* larvae are highlighted by arrows. (B) Overview of the trap formation in the $\Delta sipC$ strain. The asterisks indicate traps. A vegetative hypha is highlighted by an arrow. (C) Comparison of trapping networks in WT and the $\Delta sipC$ mutant. (D) Close-up comparison of traps in the WT, the $\Delta sipC$ mutant, and the re-complemented strain. (E) Visualization of nuclei inside of traps of the WT and the $\Delta sipC$ mutant. In the WT, the nuclei were labeled by H2B-mCherry (colored in yellow). In the $\Delta sipC$ mutant, the nuclei were labeled by H2B-GFP (colored in green). The cell wall was stained by CFW (colored in magenta). 3D reconstruction.

Traps in WT usually consist of two to four compartments before fusing to the neighboring basal hypha. In contrast, compartments of the traps in the $\Delta sipC$ -deletion strain were highly elongated as in vegetative mycelium. Interestingly, the elongated trap cells often switched to a vegetative growth mode after one, or a maximum of three trap compartments, indicated by a thinner diameter of the hyphae. The change of cell fate from trap cells to normal vegetative hyphae was confirmed by expressing the ortholog of the trap-specific serine protease P12 (DFL_008096) tagged with mCherry in the WT and the $\Delta sipC$ mutant background. Serine proteases have been identified as crucial virulence factors upon exposure to nematodes, and the *A. oligospora* P12 was highly upregulated during nematode exposure (Yang et al. 2011; Zhen et al. 2018). P12-mCherry localized in dynamic spots

inside the traps of the WT and the $\Delta sipC$ mutant (Figure 7B). The change of cell fate from trap cells to normal vegetative hyphae in traps of the $\Delta sipC$ -deletion strain was indicated by the absence of fluorescent accumulations during trap morphogenesis. This change also coincided with a change in hyphal diameter (Figure 7C). Additionally, we observed dynamic spots of P12-mCherry with weaker intensities in neighboring compartments. Therefore, we visualized the promoter activity of *p12* as described above by fusing the *p12* promoter to the fluorescent reporter construct of H2B-mCherry and transformed the plasmid into a strain expressing H2B-GFP under the control of the *h2b* promoter. Promoter activity was also present in neighboring cells but decreased in more distant vegetative hyphae (Figure 7D).

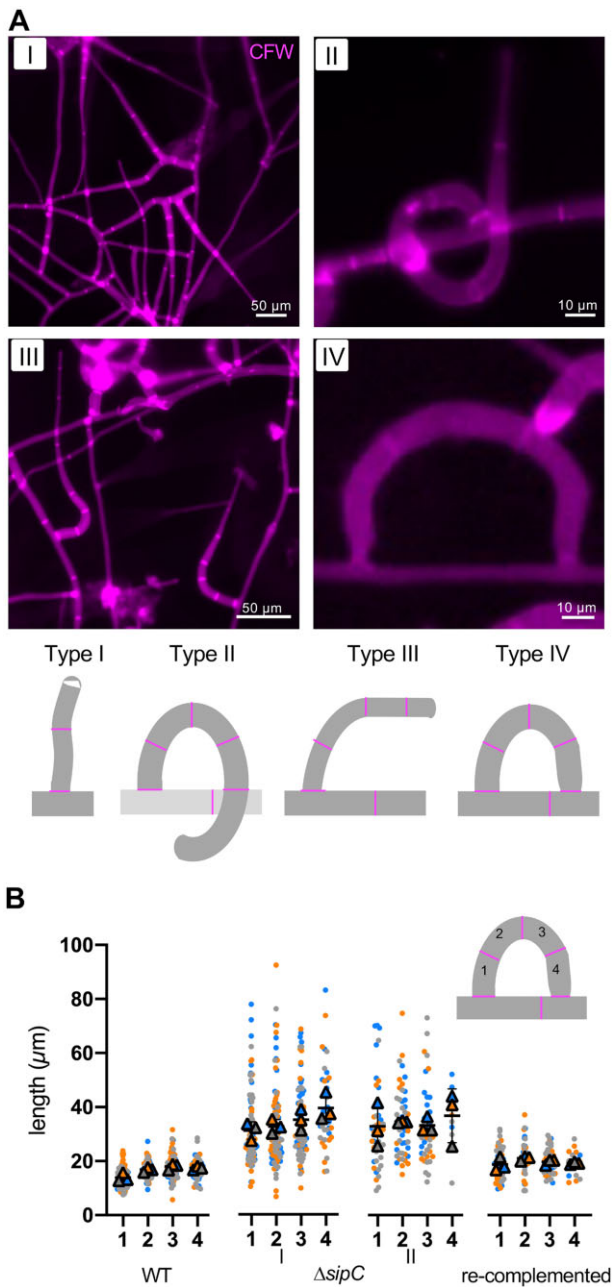


Figure 5 SipA determines trap morphology. (A) Traps of the $\Delta sipC$ mutant were divided into four groups according to their morphology. I, stick-like trap; II, ring-like trap; III, 90° bending; IV, ring with cell fusion. The cell wall was stained by CFW. (B) Quantification of the compartment length of traps in the WT, the $\Delta sipC$ mutant, and the re-complemented strain. See Table 4 for the quantification. The length of four compartments was measured. In the $\Delta sipC$ mutant, quantification of the most abundant groups I (stick-like traps) and II (ring-like traps) are displayed. Each biological replicate is color-coded (orange, blue, gray). While each data point is depicted as dot, the averages are shown as triangles. Error bars show the SD.

Since the morphology of the traps was drastically changed in the $\Delta sipC$ -deletion strain, we hypothesized that the deletion of *sipC* influences the dynamics of the cytoskeleton. The cytoskeleton has never been visualized in living traps of NTF. Therefore, we visualized MTs and F-actin by tagging the *D. flagrans* alpha-tubulin TubA with mCherry and the actin-binding peptide

Table 4 Comparison of trap compartment length in the $\Delta sipC$ -deletion strain, WT, and the re-complemented strain. Each value is displayed as mean \pm SD

$\Delta sipC$	Compartment length (in μm)				Occurrence (in %)
	1	2	3	4	
I	31 \pm 3	32 \pm 3	35 \pm 4	39 \pm 5	77 \pm 2
II	33 \pm 8	34 \pm 1	33 \pm 3	37 \pm 10	13 \pm 3
III	28 \pm 3	32 \pm 11	34 \pm 6	48 \pm 11	8 \pm 1
IV	31 \pm 9	33 \pm 6	32 \pm 12	—	1 \pm 1
WT	14 \pm 2	17 \pm 1	18 \pm 1	17 \pm 1	—
Re-compl.	19 \pm 2	21 \pm 1	20 \pm 1	19 \pm 1	—

LifeAct with GFP. In filamentous fungi, the minus ends of MTs locate at spindle pole bodies which serve as MT-organizing centers (MTOC). Additionally, areas close to the septum can act as septal MTOC (sMTOC) (Zekert et al. 2010; Gao et al. 2019). In the tip compartments, we observed dynamic MTs reaching the hyphal tip (Figure 8A). In trap cells, the most visible MTs nucleated from septal MTOCs (Figure 8A). Interestingly, major bending of the trap cell was only visible after the first septum at the base (Figure 8, B and C). Although MTs were dynamic, long MTs were observed at the inner side of the trap, reaching from the septum to the tip. In the $\Delta sipC$ mutant, MT localization appeared similar (Figure 8D). To study the role of MTs during trap morphogenesis, we added cytoskeleton-destabilizing drugs during trap development. The presence of benomyl (5 $\mu\text{g}/\text{ml}$) led to hyperbranching of the mycelium (Figure 8E). Hyphal growth during trap development stopped after the addition of benomyl (Figure 8F). Depolymerization of MTs was confirmed by imaging mCherry-labeled MTs after the addition of benomyl (Figure 8G).

Next, we visualized actin using the actin-binding peptide LifeAct-GFP (Riedl et al. 2008). Mostly, actin patches at the hyphal tip and subapical regions as well as the actomyosin ring during septum formation were visualized (Figure 9, A and B). Rarely, dynamic actin cables at the apex of hyphae were observed. Expression of Lifeact-GFP in the $\Delta sipC$ mutant revealed that septum formation was delayed during trap morphogenesis, resulting in elongated cells with decreasing hyphal diameter (Figure 9, C and D). The $\Delta sipC$ -deletion strain did not show any difference in the sensitivity toward cytochalasin A as compared to WT (data not shown).

To study the role of actin during trap morphogenesis, we added the F-actin-destabilizing drug cytochalasin A (5 $\mu\text{g}/\text{ml}$) during trap development, which led to swelling of hyphal tips of vegetative mycelium (Figure 9D). This effect was less obvious in growing traps; however, they continued to grow as vegetative hyphae at the end of the reaction (Figure 9E; Supplementary Movie S1). These results suggest a putative function of SipC in regulating cytoskeleton dynamics. However, we did not see apparent differences in the actin organization in the $\Delta sipC$ -deletion strain as compared to WT.

Discussion

The STRIPAK complex is involved in many cellular processes in eukaryotes. In filamentous fungi, it is important for hyphal fusion, sexual development, and hyphal growth (Kück et al. 2019). In this study, we show that the *D. flagrans* STRIP1/2 ortholog SipC plays a role in septation, conidiation, and trap morphogenesis

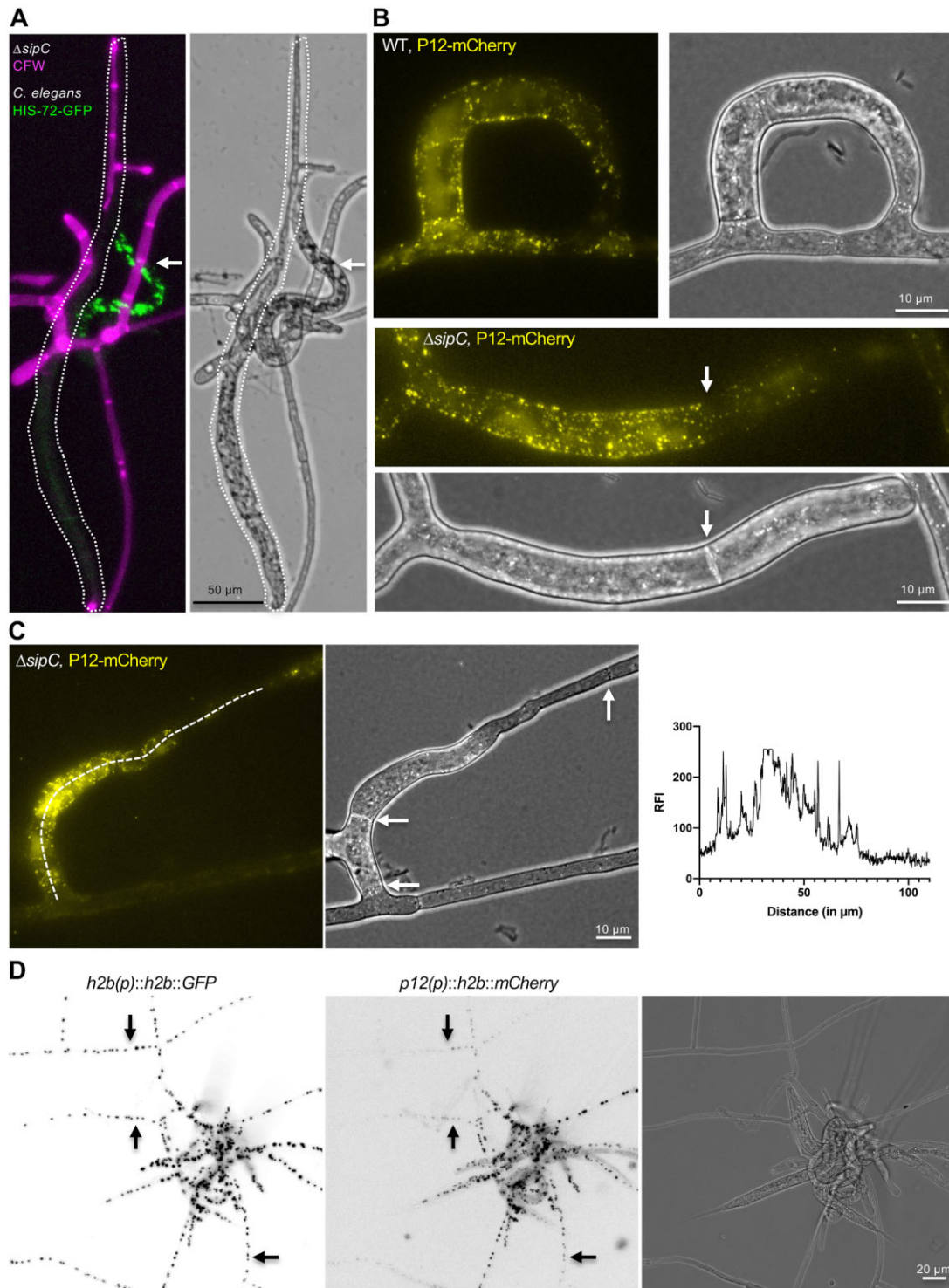


Figure 6 SipA controls the expression of trap-specific genes. (A) Trapping of *C. elegans* by traps of the $\Delta sipC$ mutant. The cell wall of the fungus is stained by CFW. A *C. elegans* strain expressing a C-terminal GFP fusion protein of the histone HIS-72 was used to distinguish between digested (surrounded by a dashed line) and trapped but alive (arrow) nematodes. (B) C-terminal mCherry tagging of the serine-protease P12 (colored in yellow) in the WT and the $\Delta sipC$ mutant. The arrow shows a septum and indicates the switch from a trap cell to vegetative growth. (C) The relative fluorescent intensity (RFI) along a $\Delta sipC$ trap was measured and plotted (x-axis displays the distance in μm ; y-axis displays the measured RFI). Arrows indicate the septa of the trap. (D) Visualization of the expression of *p12* during trapping of *C. elegans* using a H2B-mCherry reporter construct. The expression of H2B-GFP under the *h2b* promoter was used as control. Arrows indicate transition points of reduced *p12*-mCherry expression in vegetative hyphae.

and is important for cell-fate determination. Although the early steps of trap formation appeared unaffected in a *sipC*-mutant strain, trap cells apparently lost their memory and re-differentiated into normal vegetative hyphae. The same phenotype was

observed after disturbance of the actin cytoskeleton. Disturbance of the MT cytoskeleton had a completely different effect and blocked further growth of traps. There are numerous examples for the role of the STRIPAK complex in cytoskeletal functions

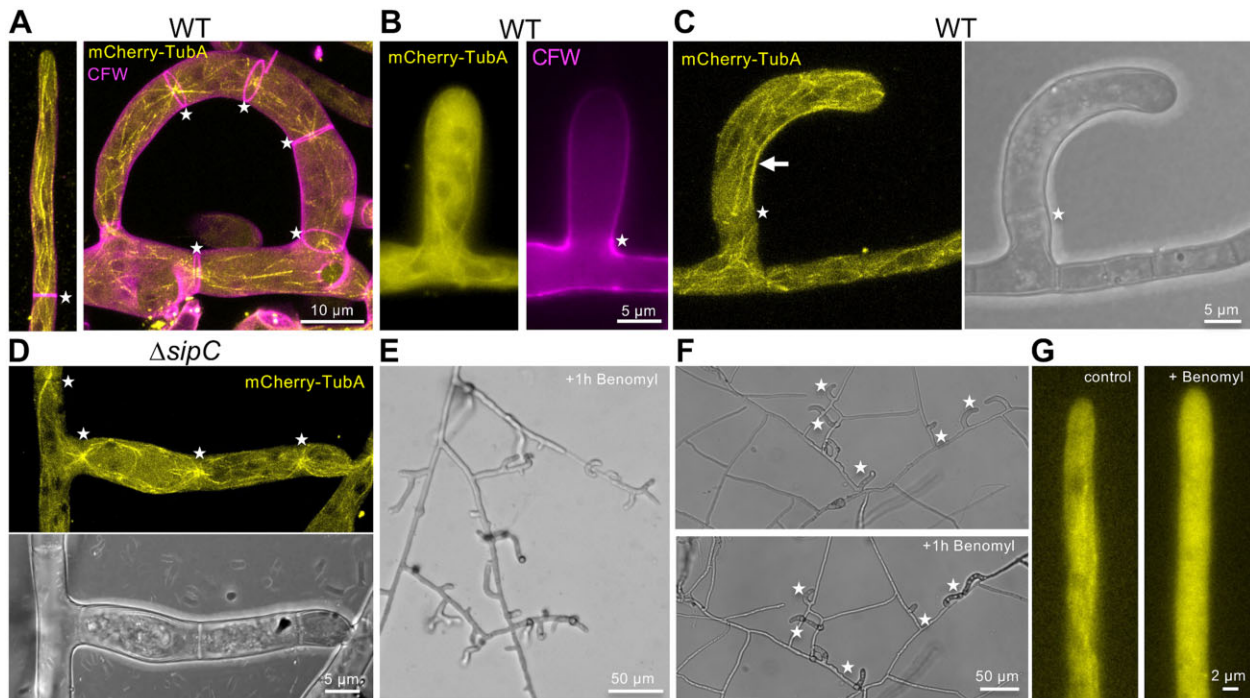


Figure 7 Characterization of the microtubule cytoskeleton. (A) Visualization of an N-terminal mCherry fusion protein of the alpha-tubulin TubA in a vegetative hypha and trap of *D. flagrans* WT (colored in yellow). The cell wall was stained by CFW (colored in magenta). Asterisks indicate the localization of septal MTOCs. Three-dimensional reconstruction. (B) Microtubules in a forming trap, where still no septum was formed at the base (asterisk). (C) MTs in a bending trap. The asterisk indicates a septal MTOC and the presence of a septum. The arrow points to microtubule bending at the inner site of the trap. (D) Localization of mCherry-TubA in a trap of the $\Delta sipC$ mutant. (E) Hyperbranching of vegetative hyphae after 1 h treatment with the microtubule-depolymerizing drug benomyl (5 $\mu\text{g}/\text{ml}$). (F) The addition of benomyl (5 $\mu\text{g}/\text{ml}$) stopped trap morphogenesis in *D. flagrans* WT. Forming traps are labeled with an asterisk. (G) Disassembly of MTs after 5 min treatment with benomyl (5 $\mu\text{g}/\text{ml}$).

(Sakuma et al. 2015). It was reported that the Strip-dependent regulation of the GCKs MST3 and MST4 modulates actomyosin contraction and therefore cell motility in cancer cells (Madsen et al. 2015). Our results raise the question of possible links among the STRIPAK signaling complex, the actin cytoskeleton, and cell-fate determination in the traps of *D. flagrans*.

In filamentous fungi, F-actin forms actin cables, rings, and patches (Berepiki et al. 2011). Actin cables are nucleated by formins and localize at the apex of hyphae, where they are involved in polar growth (Riquelme et al. 2018). Filamentous fungi usually only encode one formin and deletion of the gene in *A. nidulans* or *N. crassa* is lethal (Sharpless and Harris 2002; Justa-Schuch et al. 2010). Interestingly, the STRIPAK subunit PRO45 was found as an interaction partner of formin in *S. macrospora*, although the exact molecular function of the interaction has not yet been solved (Stein et al. 2020). It is conceivable that PRO45 influences the activity of formin. Additionally, a class II myosin was found as an interaction partner of the STRIPAK complex component PRO45 in *S. macrospora* (Nordzieke et al. 2015). The fact that *D. flagrans sipC* mutants grow very slow may reflect the role of SipC on the actin cytoskeleton in the apical dome. The effect is clearly different from the effect of cytochalasin, which destroys the actin cytoskeleton. In addition to an effect on polar growth, *sipC* mutation had a strong effect on septation. Comparable to the effect on hyphal growth, septation is still possible without SipC, but the timing appears to be different. Although this has no obvious effect on vegetative hyphae, the process appears to be crucial for trap-cell memory. A similar effect was observed during sexual development of the *S. macrospora* mutant $\Delta pro22$, where aseptated

ascogonia showed a developmental arrest at the protoperithecial stage (Bloemendal et al. 2010). This defect resulted in elongated ascogonial coils.

In addition, to a direct effect of SipC on the actomyosin system, there is good evidence in *S. pombe* that the SIN can be regulated by the STRIPAK complex. It was shown that SIP-mediated dephosphorylation of the Ste20 kinase Cdc7p initiates SIN assembly (Singh et al. 2011). Misregulation of SIP inhibits the assembly of SIN. In *A. nidulans*, the Cdc7p ortholog SepH is required for initiation of septation prior to actin ring assembly. While downregulation of *sepH* results in a loss of septation, overexpression results in hyper-septation (Bruno et al. 2001). A similar phenotype was observed in *S. macrospora* in a *Smkin3* mutant. *Smkin3* is the ortholog of *A. nidulans* SepL, and the downstream target of SepH (Radchenko et al. 2018). In this study, the deletion of the STRIPAK-complex component *sipC* resulted in a drastic reduction of septa and trap compartments of very different sizes.

Taken together, there are multiple links how SipC may affect the actin cytoskeleton and septation. Compartment size appears to be very important for cell-fate determination during trap formation.

Data availability

Strains and plasmids are available upon request. The authors affirm that all data necessary for confirming the conclusions of the article are present within the article, figures, and tables. Supplementary material is available at figshare: <https://doi.org/10.25386/genetics.16617721>.

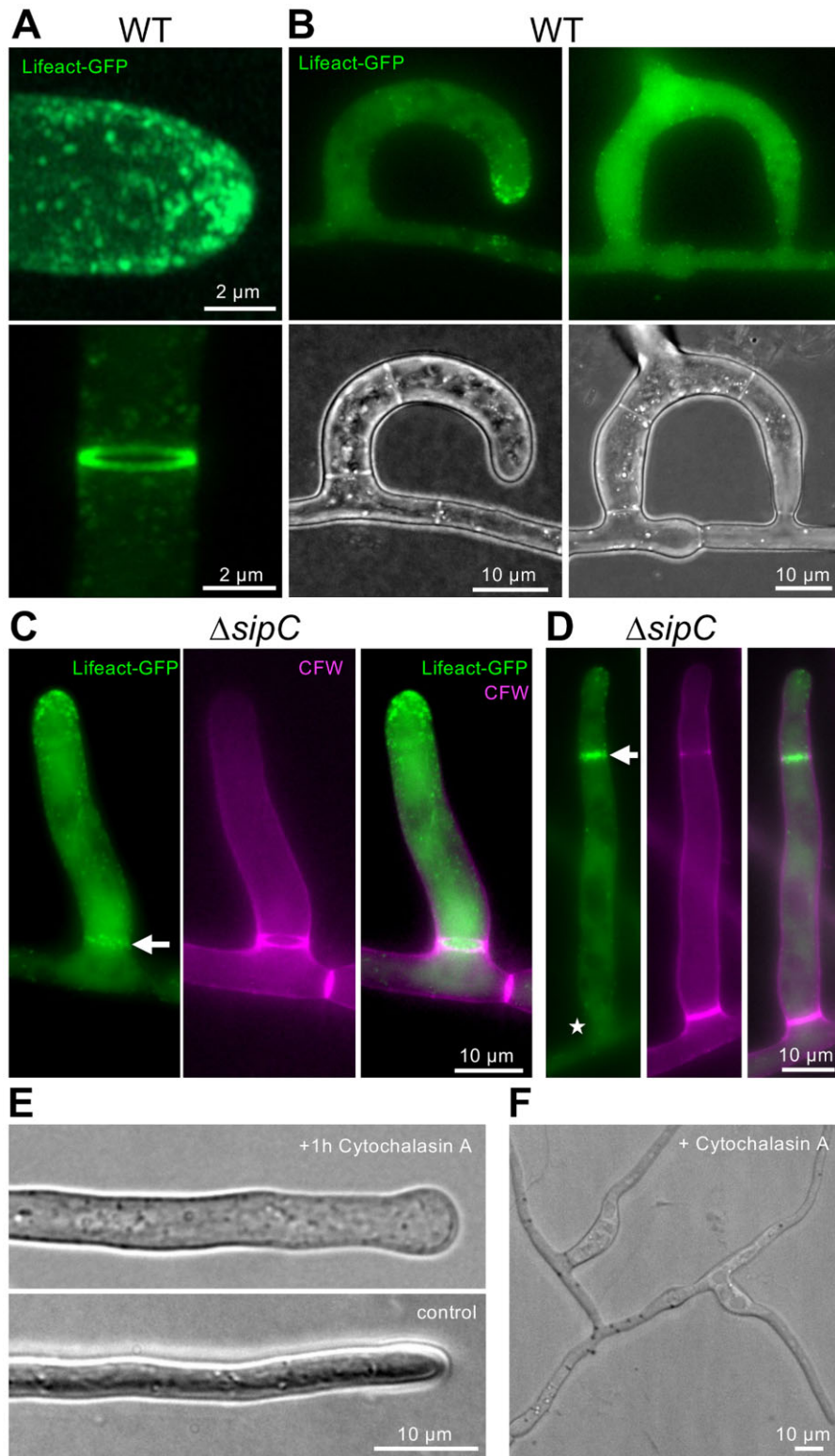


Figure 8 Characterization of the actin cytoskeleton. (A) Actin patches at a hyphal tip and an actin-ring during septum development visualized with Lifeact-GFP (colored in green). Three-dimensional reconstruction. (B) Actin during trap formation and in a mature trap. (C) Actin trap morphogenesis in the $\Delta sipC$ mutant strain. The white arrow indicates the septum at the base. The cell wall was stained by CFW. (D) Septum formation in a column-like trap in the $\Delta sipC$ mutant strain. The arrow indicates septum development by localization of Lifeact-GFP at a developing septum. The asterisk indicates a mature septum without GFP signal. (E) The addition of the actin-depolymerizing drug cytochalasin A (5 $\mu\text{g/ml}$) leads to swollen hyphal tips. As solvent control, hyphae were treated with 0.5% DMSO. (F) Loss of trap identity after the addition of cytochalasin A (5 $\mu\text{g/ml}$). After some time, traps continued to grow as vegetative hyphae (see also Supplementary Movie S1).

Acknowledgments

We are thankful to PD Dr. Ines Teichert (Ruhr University Bochum) for discussions of the project. We thank Gert Sonntag (Zeiss) and Prof. Dr. Sylvia Erhardt (KIT) for the opportunity and the help to use the LSM900 microscope.

Funding

V.W. was funded with a fellowship from the German Federal Environmental Foundation (DBU).

Conflicts of interests

The authors declare that there is no conflict of interest.

Literature cited

- Bai SW, Herrera-Abreu MT, Rohn JL, Racine V, Tajadura V, et al. 2011. Identification and characterization of a set of conserved and new regulators of cytoskeletal organization, cell morphology and migration. *BMC Biol.* 9:54.
- Berepiki A, Lichius A, Read ND. 2011. Actin organization and dynamics in filamentous fungi. *Nat Rev Microbiol.* 9:876–887.
- Bergs A, Ishitsuka Y, Evangelinos M, Nienhaus GU, Takeshita N. 2016. Dynamics of actin cables in polarized growth of the filamentous fungus *Aspergillus nidulans*. *Front Microbiol.* 7:682.
- Bloemendal S, Lord KM, Rech C, Hoff B, Engh I, et al. 2010. A mutant defective in sexual development produces aseptate ascogonia. *Eukaryot Cell.* 9:1856–1866.
- Bruno KS, Morrell JL, Hamer JE, Staiger CJ. 2001. SEPH, a Cdc7p orthologue from *Aspergillus nidulans*, functions upstream of actin ring formation during cytokinesis. *Mol Microbiol.* 42:3–12.
- Chen SA, Lin HC, Schroeder FC, Hsueh YP. 2021. Prey sensing and response in a nematode-trapping fungus is governed by the MAPK pheromone response pathway. *Genetics.* 217:iyaa008.
- Elramli N, Karahoda B, Sarikaya-Bayram O, Frawley D, Ulas M, et al. 2019. Assembly of a heptameric STRIPAK complex is required for coordination of light-dependent multicellular fungal development with secondary metabolism in *Aspergillus nidulans*. *PLoS Genet.* 15:e1008053.
- Gao X, Schmid M, Zhang Y, Fukuda S, Takeshita N, et al. 2019. The spindle pole body of *Aspergillus nidulans* is asymmetrical and contains changing numbers of gamma-tubulin complexes. *J Cell Sci.* 132:jcs234799.
- Goudreault M, D'Ambrosio LM, Kean MJ, Mullin MJ, Larsen BG, et al. 2009. A PP2A phosphatase high density interaction network identifies a novel striatin-interacting phosphatase and kinase complex linked to the cerebral cavernous malformation 3 (CCM3) protein. *Mol Cell Proteomics.* 8:157–171.
- Green KA, Becker Y, Fitzsimons HL, Scott B. 2016. An *Epichloe festucae* homologue of MOB3, a component of the STRIPAK complex, is required for the establishment of a mutualistic symbiotic interaction with *Lolium perenne*. *Mol Plant Pathol.* 17:1480–1492.
- Hsueh YP, Gronquist MR, Schwarz EM, Nath RD, Lee CH, et al. 2017. Nematophagous fungus *Arthrobotrys oligospora* mimics olfactory cues of sex and food to lure its nematode prey. *eLife.* 6:e20023.
- Hsueh YP, Mahanti P, Schroeder FC, Sternberg PW. 2013. Nematode-trapping fungi eavesdrop on nematode pheromones. *Curr Biol.* 23:83–86.
- Huang TY, Lee YY, Vidal-Diez de Ulzurrun G, Hsueh YP. 2021. Forward genetic screens identified mutants with defects in trap morphogenesis in the nematode-trapping fungus *Arthrobotrys oligospora*. G3 (Bethesda). 11:11.
- Hwang J, Pallas DC. 2014. STRIPAK complexes: structure, biological function, and involvement in human diseases. *Int J Biochem Cell Biol.* 47:118–148.
- Jeong BC, Bae SJ, Ni L, Zhang X, Bai XC, et al. 2021. Cryo-EM structure of the Hippo signaling integrator human STRIPAK. *Nat Struct Mol Biol.* 28:290–299.
- Jiang X, Xiang M, Liu X. 2017. Nematode-trapping fungi. *Microbiol Spectr.* 5: doi: 10.1128/microbiolspec.FUNK-0022-2016.
- Justa-Schuch D, Heilig Y, Richthammer C, Seiler S. 2010. Septum formation is regulated by the RHO4-specific exchange factors BUD3 and RGF3 and by the landmark protein BUD4 in *Neurospora crassa*. *Mol Microbiol.* 76:220–235.
- Kemp HA, Sprague GF, Jr. 2003. Far3 and five interacting proteins prevent premature recovery from pheromone arrest in the budding yeast *Saccharomyces cerevisiae*. *Mol Cell Biol.* 23:1750–1763.
- Kück U, Radchenko D, Teichert I. 2019. STRIPAK, a highly conserved signaling complex, controls multiple eukaryotic cellular and developmental processes and is linked with human diseases. *Biol Chem.* 400:1005–1022.
- Kuo CY, Chen SA, Hsueh YP. 2020. The high osmolarity glycerol (HOG) pathway functions in osmosensing, trap morphogenesis and conidiation of the nematode-trapping fungus *Arthrobotrys oligospora*. *J Fungi (Basel).* 6:191.
- Lord SJ, Velle KB, Mullins RD, Fritz-Laylin LK. 2020. SuperPlots: communicating reproducibility and variability in cell biology. *J Cell Biol.* 219:e202001064.
- Madsen CD, Hooper S, Tozluoglu M, Bruckbauer A, Fletcher G, et al. 2015. STRIPAK components determine mode of cancer cell migration and metastasis. *Nat Cell Biol.* 17:68–80.
- Märker R, Blank-Landeshammer B, Beier-Rosberger A, Sickmann A, Kück U. 2020. Phosphoproteomic analysis of STRIPAK mutants identifies a conserved serine phosphorylation site in PAK kinase CLA4 to be important in fungal sexual development and polarized growth. *Mol Microbiol.* 113:1053–1069.
- Mata J, Nurse P. 1997. *tea1* and the microtubular cytoskeleton are important for generating global spatial order within the fission yeast cell. *Cell.* 89:939–949.
- Niu XM, Zhang KQ. 2011. *Arthrobotrys oligospora*: a model organism for understanding the interaction between fungi and nematodes. *Mycology.* 2:59–78.
- Nordziede S, Sobel T, Franzel B, Wolters DA, Kück U, et al. 2015. A fungal sarcolemmal membrane-associated protein (SLMAP) homolog plays a fundamental role in development and localizes to the nuclear envelope, endoplasmic reticulum, and mitochondria. *Eukaryot Cell.* 14:345–358.
- Pöggeler S, Kück U. 2004. A WD40 repeat protein regulates fungal cell differentiation and can be replaced functionally by the mammalian homologue striatin. *Eukaryot Cell.* 3:232–240.
- Pracheil T, Thornton J, Liu Z. 2012. TORC2 signaling is antagonized by protein phosphatase 2A and the Far complex in *Saccharomyces cerevisiae*. *Genetics.* 190:1325–1339.
- Radchenko D, Teichert I, Pöggeler S, Kück U. 2018. A Hippo pathway-related GCK controls both sexual and vegetative developmental processes in the fungus *Sordaria macrospora*. *Genetics.* 210:137–153.
- Read ND, Beckett A. 1996. Ascus and ascospore morphogenesis. *Myc Res.* 100:1281–1314.
- Ribeiro PS, Josue F, Wepf A, Wehr MC, Rinner O, et al. 2010. Combined functional genomic and proteomic approaches identify a PP2A complex as a negative regulator of Hippo signaling. *Mol Cell.* 39:521–534.

- Riedl J, Crevenna AH, Kessenbrock K, Yu JH, Neukirchen D, et al. 2008. Lifeact: a versatile marker to visualize F-actin. *Nat Methods*. 5:605–607.
- Riquelme M, Aguirre J, Bartnicki-García S, Braus GH, Feldbrügge M, et al. 2018. Fungal morphogenesis: from the polarized growth of hyphae to complex reproduction and infection structures. *Microbiol Mol Biol Rev*. 82:e00068-17.
- Riquelme M, Bartnicki-García S, González-Prieto JM, Sánchez-León E, Verdín-Ramos JA, et al. 2007. Spitzenkörper localization and intracellular traffic of green fluorescent protein-labeled CHS-3 and CHS-6 chitin synthases in living hyphae of *Neurospora crassa*. *Eukaryot Cell*. 6:1853–1864.
- Rohn JL, Sims D, Liu T, Fedorova M, Schock F, et al. 2011. Comparative RNAi screening identifies a conserved core metazoan actinome by phenotype. *J Cell Biol*. 194:789–805.
- Sakuma C, Okumura M, Umehara T, Miura M, Chihara T. 2015. A STRIPAK component Strip regulates neuronal morphogenesis by affecting microtubule stability. *Sci Rep*. 5:17769.
- Schultzhaus Z, Quintanilla L, Hilton A, Shaw BD. 2016. Live cell imaging of actin dynamics in the filamentous fungus *Aspergillus nidulans*. *Microsc Microanal*. 22:264–274.
- Sharpless KE, Harris SD. 2002. Functional characterization and localization of the *Aspergillus nidulans* formin SEPA. *Mol Biol Cell*. 13:469–479.
- Simanis V. 2015. Pombe's thirteen—control of fission yeast cell division by the septation initiation network. *J Cell Sci*. 128:1465–1474.
- Singh NS, Shao N, McLean JR, Sevugan M, Ren L, et al. 2011. SIN-inhibitory phosphatase complex promotes Cdc11p dephosphorylation and propagates SIN asymmetry in fission yeast. *Curr Biol*. 21:1968–1978.
- Stein V, Blank-Landeshammer B, Muntjes K, Marker R, Teichert I, et al. 2020. The STRIPAK signaling complex regulates dephosphorylation of GUL1, an RNA-binding protein that shuttles on endosomes. *PLoS Genet*. 16:e1008819.
- Su H, Zhao Y, Zhou J, Feng H, Jiang D, et al. 2017. Trapping devices of nematode-trapping fungi: formation, evolution, and genomic perspectives. *Biol Rev Camb Philos Soc*. 92:357–368.
- Takeshita N, Evangelinos M, Zhou L, Somera-Fajardo RA, Lu L, et al. 2017. Pulses of Ca²⁺ coordinate actin assembly and exocytosis for stepwise cell extension. *Proc Natl Acad Sci U S A*. 114:5701–5706.
- Takeshita N, Manck R, Grün N, de Vega S, Fischer R. 2014. Interdependence of the actin and the microtubule cytoskeleton during fungal growth. *Curr Opin Microbiol*. 20:34–41.
- Takeshita N, Mania D, Herrero S, Ishitsuka Y, Nienhaus GU, et al. 2013. The cell-end marker TeaA and the microtubule polymerase AlpA contribute to microtubule guidance at the hyphal tip cortex of *Aspergillus nidulans* to provide polarity maintenance. *J Cell Sci*. 126:5400–5411.
- Teichert I, Pöggeler S, Nowrousian M. 2020. *Sordaria macrospora*: 25 years as a model organism for studying the molecular mechanisms of fruiting body development. *Appl Microbiol Biotechnol*. 104:3691–3704.
- Xiang Q, Rasmussen C, Glass NL. 2002. The ham-2 locus, encoding a putative transmembrane protein, is required for hyphal fusion in *Neurospora crassa*. *Genetics*. 160:169–180.
- Yang J, Wang L, Ji X, Feng Y, Li X, et al. 2011. Genomic and proteomic analyses of the fungus *Arthrobotrys oligospora* provide insights into nematode-trap formation. *PLoS Pathog*. 7:e1002179.
- Youssar L, Wernet V, Hensel N, Yu X, Hildebrand H-G, et al. 2019. Intercellular communication is required for trap formation in the nematode-trapping fungus *Duddingtonia flagrans*. *PLoS Genet*. 15:e1008029.
- Yu X, Hu X, Pop M, Wernet N, Kirschhöfer F, et al. 2021. Fatal attraction of *Caenorhabditis elegans* to predatory fungi through 6-methyl-salicylic acid. *Nat Commun*. 12:
- Zekert N, Veith D, Fischer R. 2010. Interaction of the *Aspergillus nidulans* microtubule-organizing center (MTOC) component ApsB with gamma-tubulin and evidence for a role of a subclass of peroxisomes in the formation of septal MTOCs. *Eukaryot Cell*. 9:795–805.
- Zhang H, Mukherjee M, Kim JE, Yu W, Shim WB. 2018. Fsr1, a striatin homologue, forms an endomembrane-associated complex that regulates virulence in the maize pathogen *Fusarium verticillioides*. *Mol Plant Pathol*. 19:812–826.
- Zhen Z, Xing X, Xie M, Yang L, Yang X, et al. 2018. MAP kinase Slt2 orthologs play similar roles in conidiation, trap formation, and pathogenicity in two nematode-trapping fungi. *Fungal Genet Biol*. 116:42–50.
- Zhou L, Obhof T, Schneider K, Feldbrügge M, Nienhaus GU, et al. 2018. Cytoplasmic transport machinery of the SPF27 homologue Num1 in *Ustilago maydis*. *Sci Rep*. 8:3611.

Communicating editor: N. L. Glass